Exploring the Influence of Graphene on Antiaromaticity of Pentalene

Keerthy P. Sudhakaran[a], Alfy Benny[b], Athira T. John[a] and Mahesh Hariharan[*a]

[a]School of Chemistry, Indian Institute of Science Education and Research Thiruvananthapuram, Vithura, Thiruvananthapuram, Kerala, 695551, India.
[b]Department of Chemistry, Princeton University, Princeton, New Jersey 08544, United States.

Electronic Supplementary Information (ESI)

Contents

Section A: Computational Techniques.....S3

- Geometry Optimizations.....S3
- Nucleus Independent Chemical Shift (NICS).....S3
- Gauge Including Magnetic Induced Current (GIMIC).....S3
- Harmonic Oscillator Model of Aromaticity (HOMA).....S3
- Anisotropy of the induced current density (AICD).....S3
- Non-Covalent Interaction analysis (NCI).....S3
- Symmetry Adapted Perturbation Theory (SAPT) S4

Section B: Tables.....S5

- Table S1: $NICS_{ZZ}$ and $\Delta NICS_{ZZ}$ calculated for bare Pentalene, Pent-$Coro_{24}$ and Pent-$Coro_{54}$ systems. NICS values are in ppm.....S5
- Table S2: The diatropic, paratropic and total net GIMIC current strengths flowing through the peripheral bond of a bare pentalene molecule. GIMIC current strength units are in nA T^{-1}. Ring numbers of pentalene are shown in Figure S1a.....S5
- Table S3: The diatropic, paratropic and total net GIMIC current strengths flowing through the peripheral bonds of pentalene molecule in optimized geometry of Pent-$Coro_{24}$ system. GIMIC current strength units are in nA T^{-1}.....S5
- Table S4: The diatropic, paratropic and total net GIMIC current strengths flowing through the peripheral bonds of pentalene molecule in optimized geometry of Pent-$Coro_{54}$ system. GIMIC current strength units are nA T^{-1}.....S6

Section C: Figures.....S7

- Figure S1: Figures showing the positions of pentalene on a) Hollow site, b) Top site and c) Bridge site on graphene surface ($Coro_{24}$).....S7

- Figure S2: The diatropic, paratropic and total net GIMIC current strengths flowing through the peripheral bond of a bare pentalene molecule. GIMIC current strength units are in nA T^{-1}. Ring numbers of pentalene are shown in Figure S1a.....S7
- Figure S3: Top view of optimized structures of a) Pent-$Coro_{24}$ and b) Pent-$Coro_{54}$.....S7
- Figure S4: Side view of optimized structures of a) Pent-$Coro_{24}$ and b) Pent-$Coro_{54}$.....S8
- Figure S5: NCI plot showing weak stabilizing interactions represented as green discs a) Pent-$Coro_{24}$ and b) Pent$Coro_{54}$.....S8
- Figure S6: Schematic illustrations of NICS-X scan probes of a) Bare Pentalene b) Pent-$Coro_{24}$ and c) Pent$Coro_{54}$.....S8
- Figure S7: Schematic illustrations of NICS probes placed at 1 Å above the centroid of a) Bare pentalene, b) Pent-$Coro_{24}$ and c) Pent $Coro_{54}$.....S9
- Figure S8: Schematic illustrations of NICS-Z scan probes of a) Bare pentalene, b) Pent-$Coro_{24}$ and c) Pent-$Coro_{54}$.....S9
- Figure S9: Schematic illustrations of the placement of integration plane across the selected bond of a) Bare pentalene b) Pent-$Coro_{24}$ and Pent-$Coro_{54}$.The value of distance (d) is equal to 1.8 Å.....S9
- Figure S0: GIMIC current strength values of a) Bare pentalene b) Pent-$Coro_{24}$ and c) Pent-$Coro_{54}$.....S10

Section D: References.....S11

Section A: Computational Techniques

Geometry Optimizations: The geometries of six pentalene-graphene model systems were optimized at the B3LYP-D3(BJ)/Def2-SVP level of theory.[1–5] The B3LYP functional included with Grimme's D3 dispersion correction and Becke–Johnson (BJ) damping is widely used for the geometry optimization of non-covalently bounded systems for getting an accurate description of dispersion and other-noncovalent interactions. The B3LYP-D3(BJ) functional avoids interatomic repulsions at short distances. The geometries of monomers (bare pentalene, coronene fragments including $C_{24}H_{12}$ ($Coro_{24}$) and $C_{54}H_{18}$ ($Coro_{54}$) were optimized at wB97XD[6]/6-311+G** level of theory. All the geometry calculations were carried out with Gaussian 16 software.[7] The optimized structures and intermolecular distances of pentalene-graphene systems are shown in Figures S3 and S4.

Nucleus Independent Chemical Shift (NICS): NICS scan calculations[8–12] were carried out using Gauge Including Atomic Orbital (GIAO) method at B3LYP/6-311+G** level of theory in Gaussian 16 software. Two types of NICS scan were performed. NICS-X scan was performed at a distance of 1.7 Å above the molecular plane of pentalene with and without the presence of graphene surfaces with an interval of 0.1 Å between the ghost atoms (Figure 3a, 3b and S7).[13] NICS-Z scan was performed for a series of ghost atoms placed at a separation of 0.1 Å along the lines passing through the centroid of five-membered ring of pentalene, perpendicular to the molecular plane (Figure S8). The ghost atoms for the NICS scan were generated using the Aroma software.[14]

Gauge Including Magnetic Induced Current (GIMIC): The relationship between nuclear magnetic shielding tensor and the current density susceptibility tensor is given by Biot-Savart law. The GIMIC program calculates current density susceptibility tensor by a combination of Biot-Savart law and the analytic gradient expression for calculating NMR shielding tensors. The calculated current densities are gauge origin independent as the gauge including atomic orbitals (GIAOs) or London Atomic Orbitals (LAOs) are employed. Integration of current density through bonds gives a quantitative measure of dominating current density flow. The density matrices for GIMIC calculation were obtained via the nuclear magnetic shielding calculation done at B3LYP/6-311+G** level of theory. The magnetically induced current densities were calculated using the GIMIC program.[15–17] The direction of external magnetic field is perpendicular to the molecular plane of pentalene.

Harmonic Oscillator Model of Aromaticity (HOMA): HOMA[18–20] values for all the rings in the molecules were calculated using Multiwfn package (version 3.6) with the formula:

$$HOMA = 1 - \frac{\alpha}{n} \sum_{i=1}^{n} (R_{opt} - R_i)^2$$

Where n is the number of C-C bonds in the ring, R_i corresponds to individual C-C bond lengths, α represent an empirical constant of value 257.7 and R_{opt} represent optimum carbon-carbon bond length.

Anisotropy of the induced current density (AICD): AICD[21,22] plots were generated by applying a continuous set of gauge transformations method (CSGT) performed at B3LYP/6-311+G** level of theory. When an external magnetic field is applied to the molecular plane of the molecule, AICD plots can be employed for the visualization of the direction and density of the induced ring current. The 3D image of the conjugated electron densities with a scalar field can be visualized using the AICD method. An aromatic molecule exhibits a clockwise direction and an antiaromatic molecule exhibits a counter clockwise direction of current density.

Non-Covalent Interaction: NCI analysis[23] employs an index based on electron density and its derivatives to identify noncovalent interactions. A two-dimensional plot of reduced electron density (s) against electron density (ρ) and the critical points are associated with the troughs appearing in the plot. Reduced electron density is given by:

$$s = \frac{1}{2(3\pi^2)^{1/3}\rho^{4/3}} |\nabla\rho|$$

Noncovalent interactions occur in the real space points where these troughs appear. The sign of second derivative of $\rho(\nabla^2\rho)$ is analyzed to distinguish attractive and repulsive interactions. The noncovalent interaction regions are represented in the plot as discs with color ranging from blue (attractive) to red (repulsive) as in the VIBGYOR spectrum.

Symmetry Adapted Perturbation Theory (SAPT): SAPT(0) analysis[24] was employed to determine the non-covalent interaction energies of dimer molecules. The SAPT module of the psi4 code was employed, with aug-cc-pVDZ basis set. SAPT(0) calculations provide the contributing components of interaction energy. The results obtained from SAPT(0) analysis is a second order perturbation expansion constituting first order electrostatic and exchange energy parts and second order dispersion, induction and their exchange counterparts as the perturbation terms

$$E_{int}^{Sapt(0)} = E_{elc}^{(1)} + E_{ex}^{(1)} + E_{ind}^{(2)} + E_{ind-ex}^{(2)} + E_{dis}^{(2)} + E_{dis-ex}^{(2)}$$

Section B: Tables

Table S1: $NICS_{ZZ}$ and $\Delta NICS_{ZZ}$ calculated for bare Pentalene, Pent-$Coro_{24}$ and Pent-$Coro_{54}$ systems. NICS values are in ppm.

Molecular systems	$NICS_{ZZ}$ (1)	$NICS_{ZZ}$ (0)	$\Delta NICS_{ZZ}$ (1)	$\Delta NICS_{ZZ}$ (0)
Bare Pentalene	56.49	91.34	-	-
Pent-$Coro_{24}$	46.60	76.43	-9.89	-14.91
Pent-$Coro_{54}$	38.99	68.84	-17.50	-22.50

Table S2: The diatropic, paratropic and total net GIMIC current strengths flowing through the peripheral bond of a bare pentalene molecule. GIMIC current strength units are in nA T^{-1}. Ring numbers of pentalene are shown in Figure S1a.

Ring numbers	Diatropic contribution	Paratropic contribution	Total net current strength
C1-C2	6.76	-24.98	-18.22
C2-C3	6.73	-22.84	-16.12
C3-C4	6.97	-24.01	-17.03
C4-C5	6.44	-23.82	-17.39
C5-C6	6.76	-24.98	-18.22
C6-C7	6.73	-22.84	-16.12
C7-C8	6.97	-24.01	-17.03
C8-C1	6.44	-23.82	-17.39

Table S3: The diatropic, paratropic and total net GIMIC current strengths flowing through the peripheral bonds of pentalene molecule in optimized geometry of Pent-$Coro_{24}$ system. GIMIC current strength units are in nA T^{-1}.

Ring numbers	Diatropic contribution	Paratropic contribution	Total net current strength

C1-C2	6.99	-25.29	-18.30
C2-C3	6.96	-23.32	-16.36
C3-C4	7.10	-24.01	-16.91
C4-C5	6.53	-23.90	-17.47
C5-C6	6.84	-25.07	-18.23
C6-C7	6.70	-22.75	-16.05
C7-C8	7.09	-24.06	-16.97
C8-C1	-24.36	-24.36	-17.72

Table S4: The diatropic, paratropic and total net GIMIC current strengths flowing through the peripheral bonds of pentalene molecule in optimized geometry of Pent-Coro$_{54}$ system. GIMIC current strength units are in nA T^{-1}.

Ring Numbers	Diatropic contribution	Paratropic contribution	Total net current strength
C1-C2	6.96	-24.65	-17.69
C2-C3	6.97	-22.49	-15.52
C3-C4	7.33	-23.18	-15.87
C4-C5	6.69	-23.80	-17.11
C5-C6	7.03	-24.58	-17.56
C6-C7	7.06	-22.56	-15.50
C7-C8	7.30	-23.12	-15.71
C8-C1	6.56	-23.87	-17.31

Section C: Figures

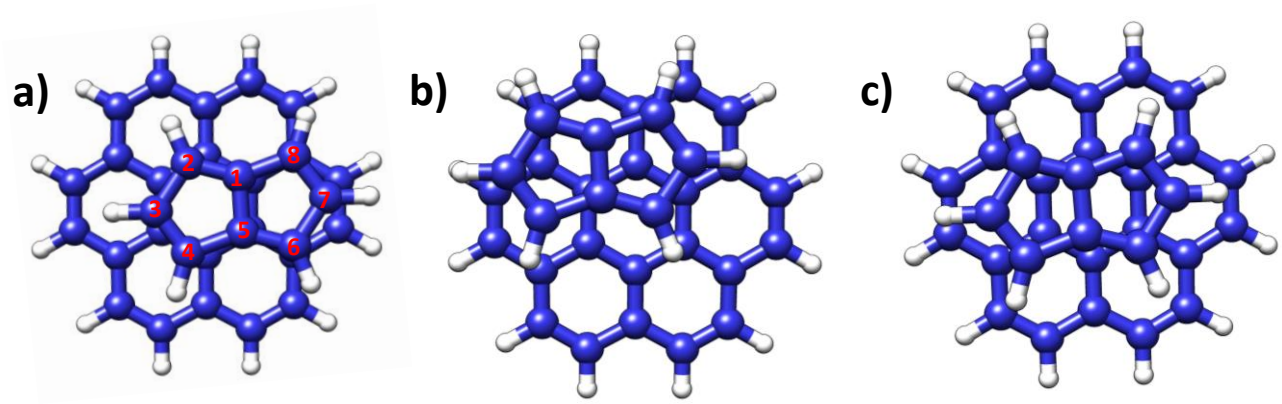

Figure S1: Figures showing the positions of pentalene on a) Hollow site, b) Top site and c) Bridge site on graphene surface ($Coro_{24}$).

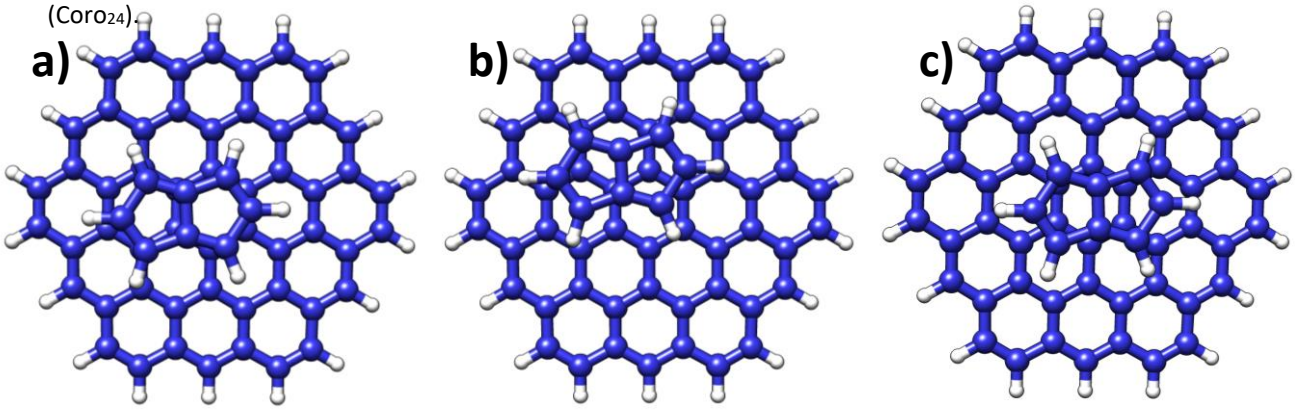

Figure S2: Figures showing the positions of pentalene on a) Hollow site, b) Top site and c) Bridge site on graphene surface ($Coro_{54}$).

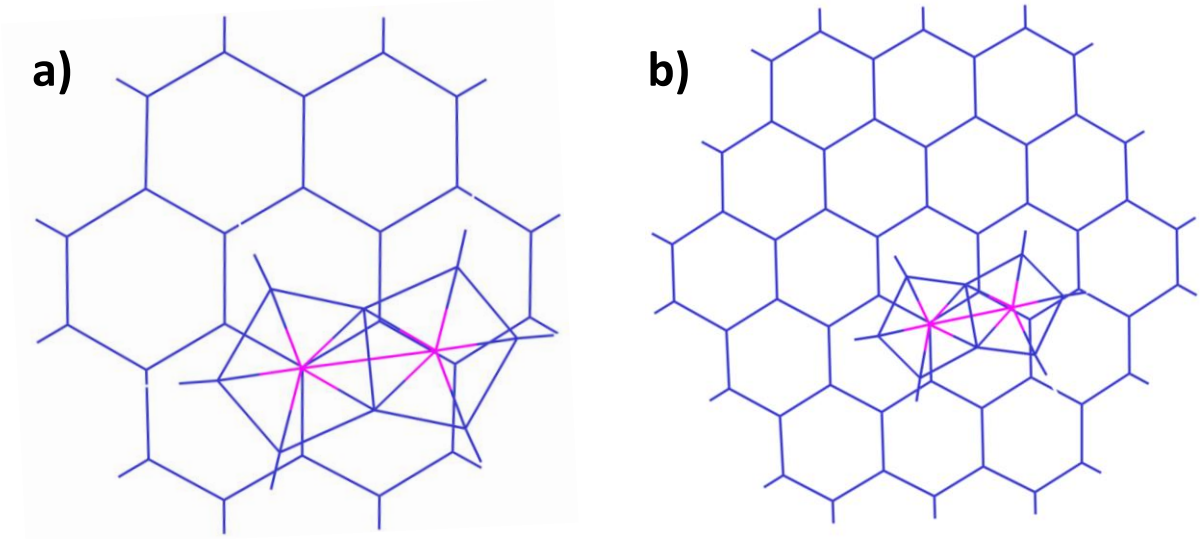

Figure S3: Top view of optimized structures of a) Pent-$Coro_{24}$ and b) Pent-$Coro_{54}$.

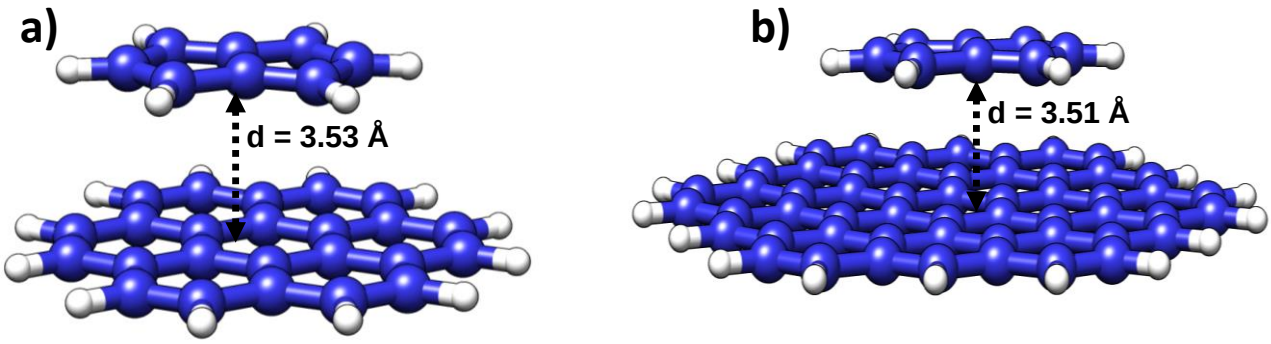

Figure S4: Side view of optimized structures of a) Pent-Coro$_{24}$ and b) Pent-Coro$_{54}$.

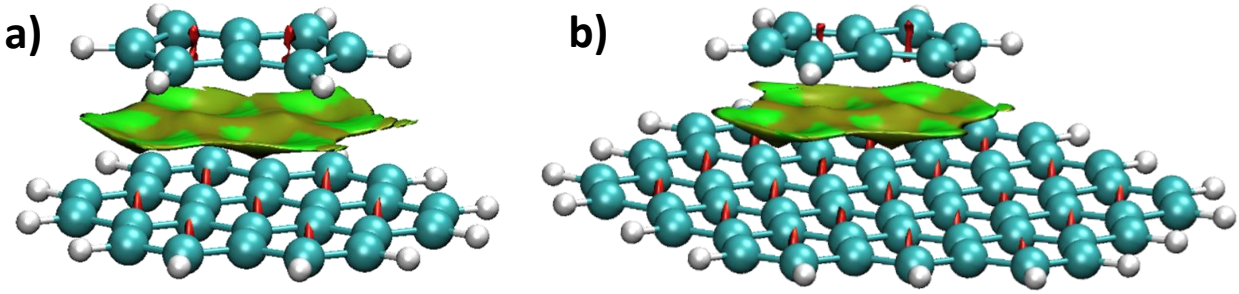

Figure S5: NCI plot showing weak stabilizing interactions represented as green discs a) Pent-Coro$_{24}$ and b) Pent-Coro$_{54}$.

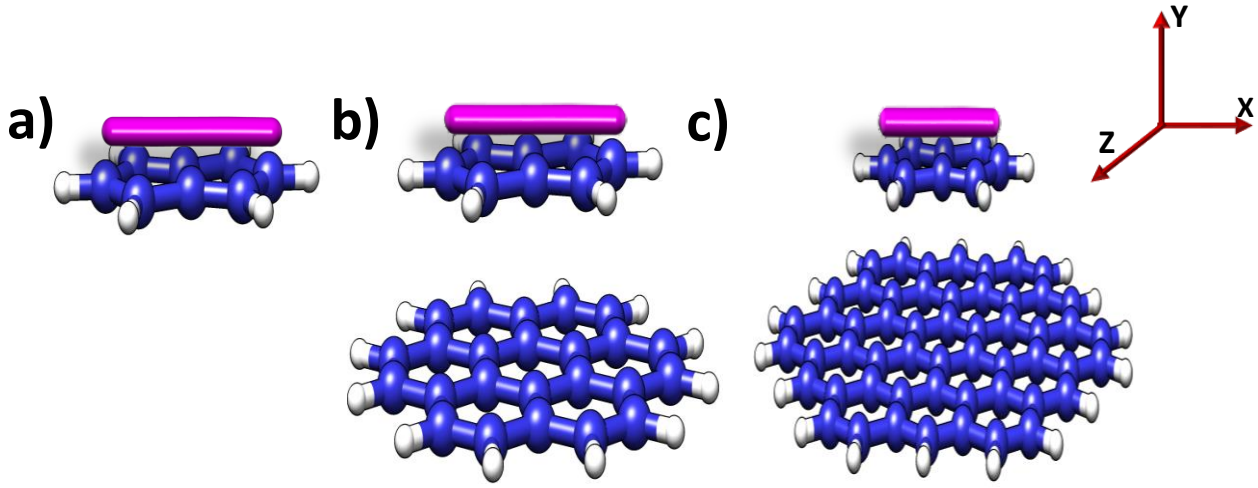

Figure S6: Schematic illustrations of NICS-X scan probes of a) Bare pentalene b) Pent-Coro24 and c) Pent-Coro54.

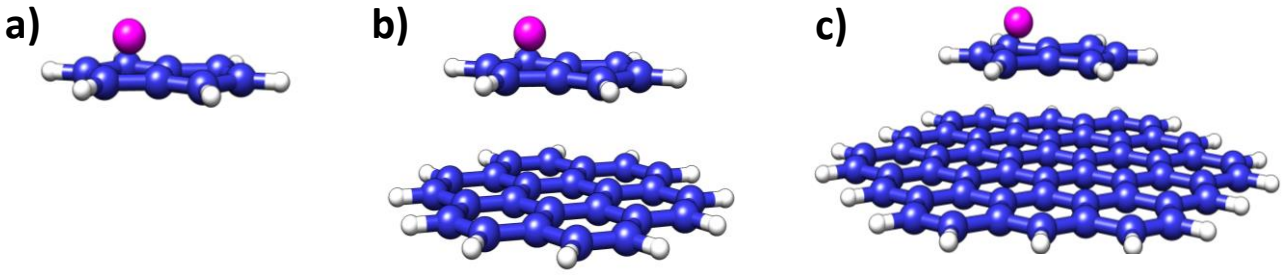

Figure S7: Schematic illustrations of NICS probes placed at 1 Å above the centroid of a) Bare pentalene, b) Pent-Coro$_{24}$ and c) Pent-Coro$_{54}$.

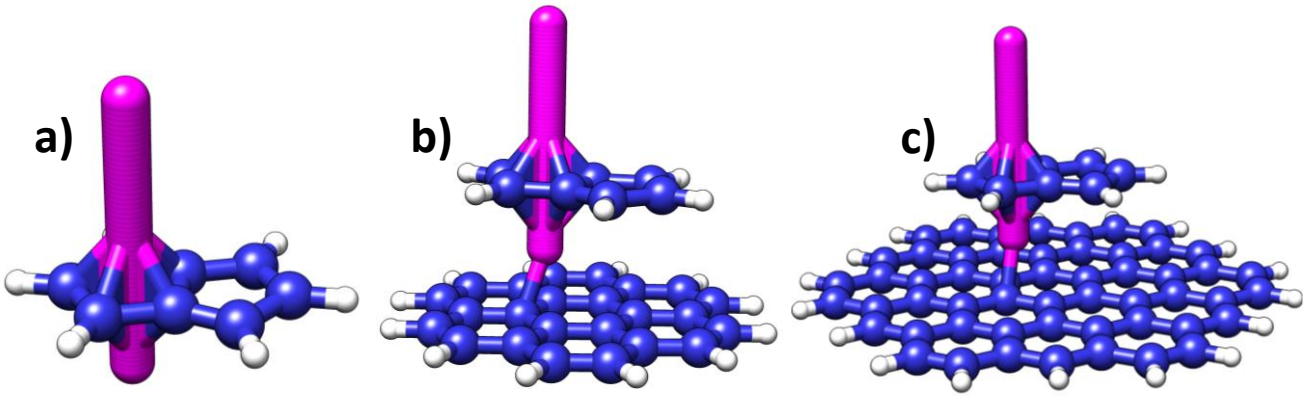

Figure S8: Schematic illustrations of NICS-Z scan probes of a) Bare pentalene, b) Pent-Coro$_{24}$ and c) Pent-Coro$_{54}$.

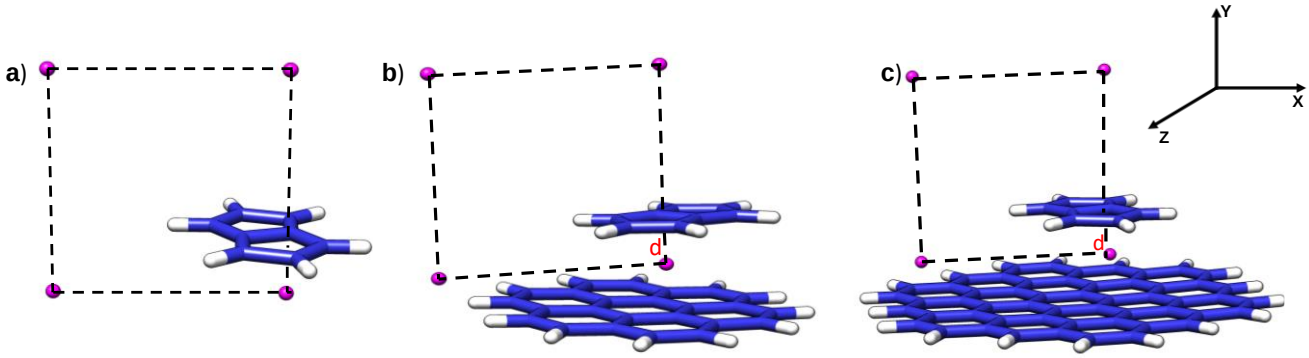

Figure S9: Schematic illustrations of the placement of integration plane across the selected bond of a) Bare pentalene b) Pent-Coro$_{24}$ and Pent-Coro$_{54}$.The value of distance (d) is equal to 1.8 Å.

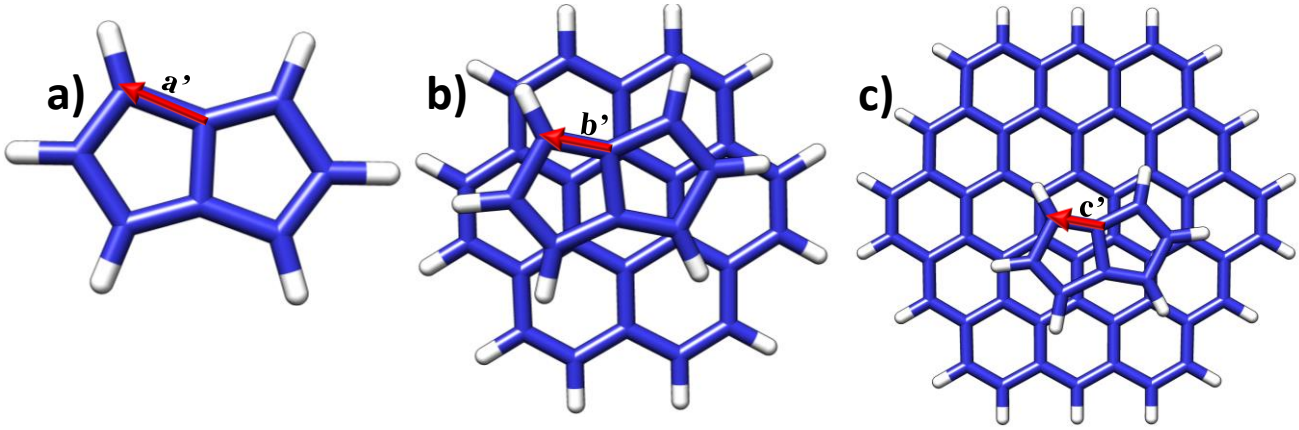

Figure S10: GIMIC current strength values of a) Bare pentalene b) Pent-Coro$_{24}$ and c) Pent-Coro$_{54}$. Values of a'=-17.19 nA T^{-1}, b'=-17.25 nA T^{-1} and c'=-16.55 nA T^{-1}.

Section D: References:

1. J. P. Perdew, K. Burke and M. Ernzerhof, *Phys. Rev. Lett.*, 1996, **77**, 3865–3868.
2. K. Raghavachari, *Theor. Chem. Acc.*, 2000, **103**, 361–363.
3. F. Weigend and R. Ahlrichs, *Phys. Chem. Chem. Phys.*, 2005, **7**, 3297–3305.
4. S. Grimme, *Wiley Interdiscip. Rev. Comput. Mol. Sci.*, 2011, **1**, 211–228.
5. A. D. Becke and E. R. Johnson, *J. Chem. Phys.*, 2005, **123**, 154101.
6. J. Da Chai and M. Head-Gordon, *Phys. Chem. Chem. Phys.*, 2008, **10**, 6615–6620.
7. M. J. Frisch, G. W. Trucks, H. B. Schlegel, G. E. Scuseria, M. a. Robb, J. R. Cheeseman, G. Scalmani, V. Barone, G. a. Petersson, H. Nakatsuji, X. Li, M. Caricato, a. V. Marenich, J. Bloino, B. G. Janesko, R. Gomperts, B. Mennucci, H. P. Hratchian, J. V. Ortiz, a. F. Izmaylov, J. L. Sonnenberg, Williams, F. Ding, F. Lipparini, F. Egidi, J. Goings, B. Peng, A. Petrone, T. Henderson, D. Ranasinghe, V. G. Zakrzewski, J. Gao, N. Rega, G. Zheng, W. Liang, M. Hada, M. Ehara, K. Toyota, R. Fukuda, J. Hasegawa, M. Ishida, T. Nakajima, Y. Honda, O. Kitao, H. Nakai, T. Vreven, K. Throssell, J. a. Montgomery Jr., J. E. Peralta, F. Ogliaro, M. J. Bearpark, J. J. Heyd, E. N. Brothers, K. N. Kudin, V. N. Staroverov, T. a. Keith, R. Kobayashi, J. Normand, K. Raghavachari, a. P. Rendell, J. C. Burant, S. S. Iyengar, J. Tomasi, M. Cossi, J. M. Millam, M. Klene, C. Adamo, R. Cammi, J. W. Ochterski, R. L. Martin, K. Morokuma, O. Farkas, J. B. Foresman and D. J. Fox, 2016, Gaussian 16, Revision C.01, Gaussian, Inc., Wallingford CT, 2016.
8. Z. Chen, C. S. Wannere, C. Corminboeuf, R. Puchta and P. von Ragué Schleyer, *Chem. Rev.*, 2005, **105**, 3842–3888.
9. A. Stanger, *European J. Org. Chem.*, 2020, 3120–3127.
10. A. Stanger, *J. Org. Chem.*, 2006, **71**, 883–893.
11. R. Gershoni-Poranne and A. Stanger, *Chem. Soc. Rev.*, 2015, **44**, 6597–6615.
12. P. V. R. Schleyer, C. Maerker, A. Dransfeld, H. Jiao and N. J. R. Van Eikema Hommes, *J. Am. Chem. Soc.*, 1996, **118**, 6317–6318.
13. A. Stanger, G. Monaco and R. Zanasi, *ChemPhysChem*, 2020, **21**, 65–82.
14. A. Rahalkar, A. Stanger, "Aroma". This software may be downloaded free of charge from http://schulich.technion.ac.il/Amnon_Stanger.htm.
15. J. Jusélius, D. Sundholm and J. Gauss, *J. Chem. Phys.*, 2004, **121**, 3952–3963.
16. S. Taubert, D. Sundholm and J. Jusélius, *J. Chem. Phys*., 2011, **134**, 054123.
17. H. Fliegl, S. Taubert, O. Lehtonen and D. Sundholm, *Phys. Chem. Chem. Phys.*, 2011, **13**, 20500–20518.
18. T. M. Krygowski and M. K. Cyrański, *Chem. Rev.*, 2001, **101**, 1385–1420.
19. T. M. Krygowski, H. Szatylowicz, O. A. Stasyuk, J. Dominikowska and M. Palusiak, *Chem. Rev.*, 2014, **114**, 6383–6422.
20. J. Kruszewski and T. M. Krygowski, *Tetrahedron Lett.*, 1972, **13**, 3839–3842.
21. D. Geuenich, K. Hess, F. Köhler and R. Herges, *Chem. Rev.*, 2005, **105**, 3758–3772.
22. R. Herges and D. Geuenich, *J. Phys. Chem. A*, 2001, **105**, 3214–3220.
23. J. Contreras-García, E. R. Johnson, S. Keinan, R. Chaudret, J.-P. Piquemal, D. N. Beratan and W. Yang, *J. Chem. Theory Comput.*, 2011, **7**, 625–632.
24. K. Szalewicz, *Wiley Interdiscip. Rev. Comput. Mol. Sci.*, 2012, **2**, 254–272.